Bifurcations of Periodic Orbits in Axisymmetric Scalefree Potentials [a]

C. Hunter,[b] Balša Terzić,[b] Amy M. Burns,[c]
Donald Porchia,[b] and Chris Zink.[b]

[b]*Department of Mathematics*
Florida State University
Tallahassee, FL 32306-4510

[c]*Department of Engineering Physics*
Embry Riddle Aeronautical University
Daytona Beach, FL 32114

ABSTRACT

We study orbits in potentials with central cusps, emphasizing the SED potentials generated by mass distributions with spheroidal equidensity surfaces. The most prominent bifurcations are those related to 1:1 and 4:3 resonances between radial motions and motions perpendicular to the central plane. We find that 1:1 resonances can cause the thin tube orbit, as well as the equatorial plane orbit, to become unstable. We concentrate on period-tripling bifurcations because they appear to be the least understood. We study them via a class of analytic maps. This study suggests that stable period-three orbits generally arise *de novo* in stable and unstable pairs via a turning-point bifurcation, and not through a bifurcation from the thin tube at a 120° rotation angle. The stable period-three orbits typically have only a short span of existence before becoming unstable to a period-doubling instability through a supercritical pitchfork bifurcation.

1. INTRODUCTION

An understanding of orbits is essential to an understanding of the dynamical structure of elliptical galaxies. Elliptical galaxies are believed to be composed primarily of stars moving collisionlessly, because two-body encounters are rare, in their own gravitational fields. The orbits of these stars therefore are the building blocks from which a dynamical

[a] This work has been supported in part by National Science Foundation Grants DMS-9304012 and 9704615, and by the Florida Space Grant Consortium.

model for a galaxy is constructed.

This paper is concerned with orbits in a special class of such gravitational fields, those arising from scalefree potentials for which the potential varies as some power $-\beta$ of distance from the center. The dynamics is then simplified because the range of orbits that is possible at any one energy is geometrically similar to the range that is possible at any other energy.[1] This feature, which obviously simplifies the task of surveying the full range of orbits, has been one reason for studying dynamics in scalefree potentials. Another reason is that scalefree potentials allow naturally for the presence of a central density cusp. HST observations have shown that cusps are a common feature of early-type elliptical galaxies, and that some appear even to have nearly pure power-law profiles.[2]

A wide variety of potentials remain even with the simplifying restriction to scalefree. That is because the scalefree property places no restriction on the manner in which the potential varies on a spherical surface centered on the cusp; it requires only that this variation be the same at all radii. We restrict this variation very considerably in focussing on SEP and SED potentials. SEP and SED are mnemonics for spheroidal equipotential and spheroidal equidensity. Because equipotentials are always rounder than the equidensity surfaces of the underlying mass distribution that give rise to the potential, that mass distribution can become quite extreme with spheroidal equipotentials.[1] Specifically regions of negative density arise on the axis of symmetry if

$$q^2 < \frac{1}{2}(1+\beta), \tag{1}$$

and in the equatorial plane if

$$\frac{1}{q^2} < \beta. \tag{2}$$

Here q is the ratio of the axis of the equipotential spheroid along the axis of symmetry to that perpendicular to it. These spheroids are oblate if $q < 1$, prolate if $q > 1$, and spherical if $q = 1$. Inequalities (1) and (2) allow a range of possibilities with everywhere positive densities for $\beta < 1$, that is for potentials less singular than that of a point mass. Evans's[1] Figure 1(a) displays a more restricted region of parameter space. That is because he has imposed the extra requirement of a positive phase-space density of the unique two-integral distribution function. Earlier surveys, as well as the present one, show considerable evidence for the existence of a third integral of motion on which the distribution function can, and probably does, depend. Hence the region of parameter space for which there are distribution functions with everywhere positive phase-space densities is likely larger.

By construction, SED potentials arise from everywhere positive mass densities. As FIGURE 6 of Qian *et al* [3] shows, the extra requirement of positive phase-space density of the two-integral distribution function restricts their parameter space too. Our survey of these models shows that they too generally have third integrals and hence a much greater variety of possible distribution functions. We carry out our survey for each family by selecting values of the parameters β and q, while choosing the representative value of the energy to be that for which the maximum magnitude of the angular momentum L_z about the axis of symmetry is $1/\sqrt{e} = .6065$. This choice gives the same range of L_z as in Richstone's pioneering investigation of orbits in the logarithmic SEP.[4] We then study the dynamics of the orbits at lesser values of L_z by constructing surfaces of section. Our main interest here is to determine the types of orbits that occur, the constraints to which they are subject in phase space, and the formation of new classes of orbits that arise through bifurcations.

Section 2 gives basic definitions and equations. Section 3 describes some of the more significant findings of our survey. The bifurcations that are least understood, though among the most prominent, are period-tripling ones. Section 4 describes a class of maps constructed specifically to model period-tripling bifurcations, and which are helpful in understanding their occurrence in this and other work. Section 5 summarizes our results and draws conclusions.

2. SCALEFREE AXISYMMETRIC POTENTIALS

2.1. Potentials

We follow Binney & Tremaine[5] in using $r = \sqrt{x^2 + y^2 + z^2}$ to denote distance in spherical coordinates, and $R = \sqrt{x^2 + y^2}$ to denote distance from the z-axis of symmetry.

Any axisymmetric potential of the form

$$\Phi = \frac{F(\theta)}{r^\beta}, \tag{3}$$

where θ is a colatitude angle measured from the axis of symmetry and F is an arbitrary function, is scalefree. We restrict attention to potentials with reflective symmetry with respect to the central $z = 0$ plane so that

$$\Phi(R, -z) = \Phi(R, z), \tag{4}$$

and hence the function $F(\theta)$ of equation (3) has the reflective symmetry

$$F(\theta) = F(\pi - \theta), \tag{5}$$

about $\theta = \pi/2$. We normalize the spheroidal equipotential (SEP) to the form

$$\Phi(R, z) = \frac{-1}{\beta[R^2 + z^2/q^2]^{\beta/2}} = -\frac{1}{\beta r^\beta}\left[\sin^2\theta + \frac{\cos^2\theta}{q^2}\right]^{-\beta/2}, \tag{6}$$

The logarithmic SEP potential

$$\Phi(R, z) = \frac{1}{2}\ \ln\left[R^2 + \frac{z^2}{q^2}\right], \tag{7}$$

studied by Richstone[4] is obtained as the $\beta \to 0$ limit of $(\Phi + \beta^{-1})$ for the Φ of (6), the added constant, which has no effect on the derivatives of Φ which give the forces, is needed to obtain a finite limit as $\beta \to 0$. The more general $\beta \neq 0$ cases of (6) were studied by Evans.[1]

The SED scalefree potentials that arise from a mass distribution with spheroidal equidensity surfaces are defined implicitly by Poisson's equation

$$\nabla^2\Phi = \frac{4\pi G\rho_0}{[R^2 + z^2/q^2]^{1+\beta/2}}, \tag{8}$$

where ρ_0 is the density at $R = 1$, $z = 0$. The function $F(\theta)$ now has a more complicated form that involves elliptic integrals.[6] Because it time consuming and computationally inefficient to have to evaluate these integrals at each step of an orbit, we first derive Fourier series representations, which are of the form

$$F(\theta) = \frac{1}{2}B_0 + \sum_{j=1}^{\infty} B_j \cos 2j\theta, \tag{9}$$

because of the symmetry (5). The B_j coefficients depend on β and q, and must be computed anew for each potential. That is a simple task because the integrals that define the coefficients integrate a periodic integrand over a complete period. Hence a simple repeated trapezoidal rule suffices.[7] Few Fourier coefficients are needed to achieve high accuracy, except as $q \to 0$, because $F(\theta)$ is analytic and the $B_j(q,\beta)$ consequently decay exponentially with j for large j.[8] To aid comparisons, we choose ρ_0 in (8) such that $F(\pi/2) = -1/\beta$. Then the values of both SED and SEP potentials are

$$\Phi(R,0) = -\frac{1}{\beta R^\beta}, \tag{10}$$

in the central plane $z = 0$.

2.2. Dynamics of Orbits

The angular momentum

$$L_z = R^2 \dot{z}, \tag{11}$$

of any orbit about the z-axis of symmetry is conserved, because the potential is axisymmetric. The equations of motion for the orbit are

$$\ddot{R} = \frac{L_z^2}{R^3} - \frac{\partial \Phi}{\partial R}, \quad \ddot{z} = -\frac{\partial \Phi}{\partial z}, \tag{12}$$

and can be solved without explicitly considering motion in the longitudinal angle. The orbit has an energy integral

$$\frac{1}{2}\big(\dot{R}^2 + \dot{z}^2 + \frac{L_z^2}{R^2}\big) + \Phi(R,z) = E. \tag{13}$$

The orbit that lies always in the equatorial plane $z = 0$ is found by integrating the $z \equiv 0$ form of the energy integral:

$$\dot{R}^2 = 2E + \frac{2}{\beta R^\beta} - \frac{L_z^2}{R^2}. \tag{14}$$

This expression for $\dot{R}^2$ has a unique maximum at $R^{2-\beta} = L_z^2$. When this maximum is zero, that is when $E = (\frac{1}{2} - \frac{1}{\beta})L_z^{-2\beta/(2-\beta)}$, then the only possible orbit is a circular orbit in

$z = 0$. We use the freedom given by the scalefree nature of the potential to fix the energy at

$$E = \left(\frac{1}{2} - \frac{1}{\beta}\right) e^{\frac{\beta}{2-\beta}}, \tag{15}$$

so that all other orbits occur only in the range

$$0 \leq L_z^2 < \frac{1}{e} = .3679. \tag{16}$$

2.3. Surfaces of Section

We study $z = 0$ surfaces of section of orbits, marking crossings in the $(R, \dot{R})$-plane at which the section is crossed with $\dot{z} > 0$. The value of $\dot{z}$ at a crossing is known to be

$$\dot{z} = \sqrt{\left(1 - \frac{2}{\beta}\right) e^{\frac{\beta}{2-\beta}} - \dot{R}^2 + \frac{2}{\beta R^\beta} - \frac{L_z^2}{R^2}} \tag{17}$$

from the energy integral (13). Each surface of section is finite and is bounded by the $\dot{z} = 0$ curve that is the locus (14) of the equatorial plane orbit. We explore the surface of section by integrating, for sufficiently long times, orbits that start from a selected range of feasible positions in the $(R, \dot{R})$-plane with the initial value (17).

3. ORBITAL SURVEYS AND BIFURCATIONS

Our survey has included both oblate and prolate SEP and SED potentials, which we study for decreasing values of L_z^2 in the range (16). The power β has largely been restricted to the range $-.5 \leq \beta \leq .5$, which includes both rising ($\beta < 0$) and falling ($\beta > 0$) rotation curves. All potentials in this β-range arise from density distributions that have an $R^{-1-\beta}$ cusp when seen in projection.

3.1. Orbits at High Angular Momenta

Surfaces of section can be understood analytically when L_z^2 is only slightly less than its maximum $1/e$. Orbits then depart little from circular. The equations of motion (12), linearized about an $R = R_0 = L_z^{2/(2-\beta)}$, $z = 0$, circular orbit are

$$\ddot{R} + \kappa^2 (R - R_0) = 0,$$

$$\ddot{z} + \nu^2 z = 0.$$

Here the constants κ and ν, defined via the equations

$$\kappa^2 = \frac{\partial^2 \Phi}{\partial R^2} + \frac{3}{R}\frac{\partial \Phi}{\partial R}\bigg|_{\substack{R=R_0 \\ z=0}} = \frac{2-\beta}{R_0^{\beta+2}}, \quad \nu^2 = \frac{\partial^2 \Phi}{\partial z^2}\bigg|_{\substack{R=R_0 \\ z=0}} = \frac{F''(\pi/2) - \beta F(\pi/2)}{R_0^{\beta+2}}, \tag{18}$$

are respectively the epicyclic and perpendicular out-of-plane frequency for the potential in the equatorial plane. The generic orbit crosses the surface of section at

$$R - R_0 = \frac{C}{\kappa} \sin\left[\frac{2n\pi\kappa}{\nu} + \chi\right], \quad \dot{R} = C \cos\left[\frac{2n\pi\kappa}{\nu} + \chi\right], \tag{19}$$

for integers $n \geq 0$ and constants C and χ; that is at a sequence of points that lie on an ellipse. The surface of section is bounded by a largest ellipse for which $C = [2E + ((1/\beta) - 1)R_0^{-\beta}]^{1/2}$ and there is a single point at its center at which the orbit whose perturbation from circular is solely in z-motion crosses repeatedly. If the ratio κ/ν is irrational, then the succession of crossing points generated by a single orbit does not repeat, and continues to fill in the outline of the ellipse. The crossing points do repeat when κ/ν is rational and the orbit is periodic.

Figure 1(a) shows a surface of section that is typical of relatively high angular momenta. It is qualitatively similar, indeed topologically equivalent, to that given by equations (19) for nearly circular orbits, even though $L_z^2 = 0.1$ here is well below the maximum of e^{-1}. The periodic orbit represented by the fixed point of the surface of section at $R = 0.54$, $\dot{R} = 0$ is a thin tube orbit. As Figure 1(b) shows, it is confined to a curve in (R, z)-space, and oscillates in R as well as z. The loci of crossings of individual orbits lose their elliptical shape away from the central fixed point, but they are still familially related to the thin tube orbit. They are now confined to fat tubes, with non-zero cross-sectional area in (R, z)-space, that encircle the z-axis of symmetry,

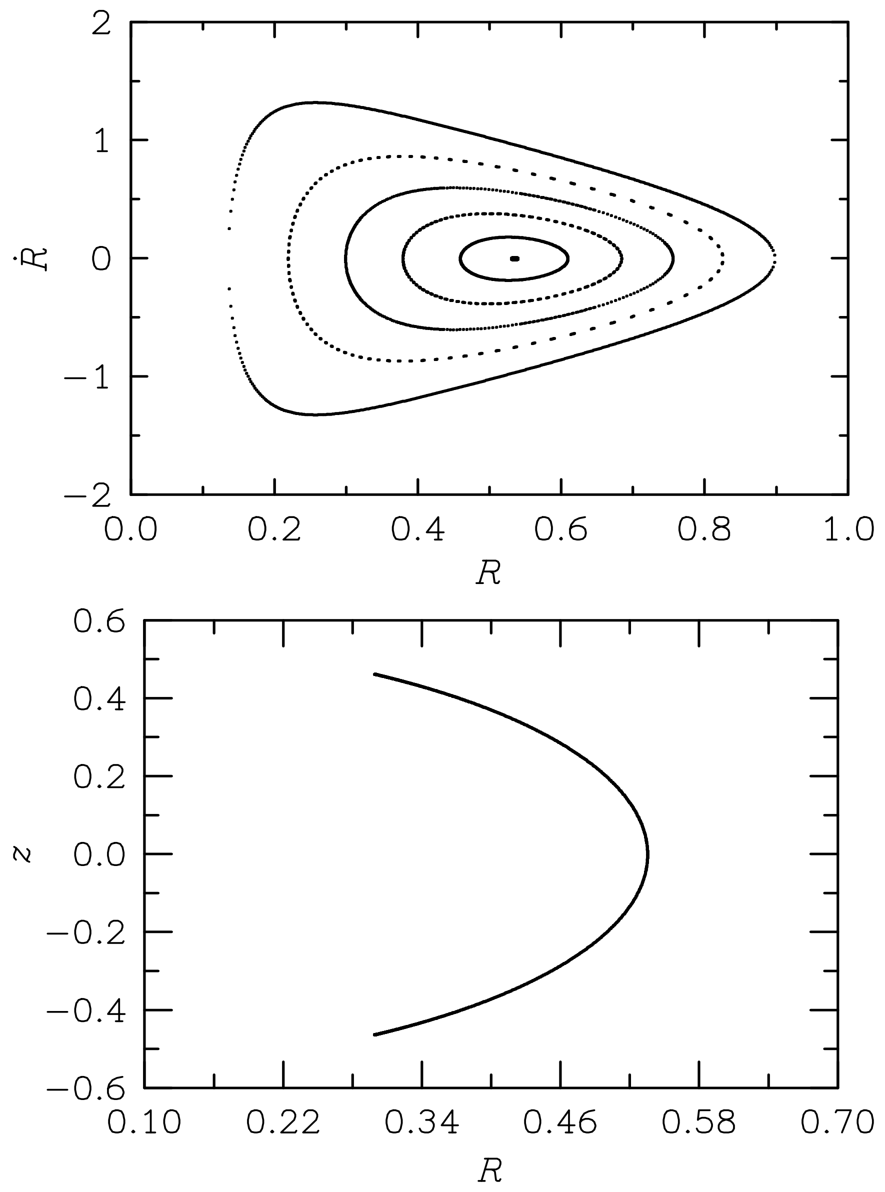

FIGURE 1. (**a**) The $(R, \dot{R})$ surface of section for an oblate SED potential ($q = 0.8, \beta = 0.3$) with $L_z^2 = 0.1$. (**b**) The path in (R, z) space of the thin tube orbit represented by the central point of the surface of section.

3.2. Bifurcations

3.2.1. Instability of the Equatorial Plane Orbit

The most prominent bifurcation seen in previous work on SEP potentials[1,4,9] is that due to a 1:1 resonance between the nonlinear oscillation in R of the equatorial plane orbit and a small oscillation in z. It causes that previously stable orbit to become unstable at the critical value of $L_z^2 = 0.0485$ for the SEP potential of FIGURE 2, and to be replaced by the pair of stable banana orbits. FIGURE 2(a) shows the surface of section at the lower value of $L_z^2 = 0.01$, and FIGURE 2(b) shows the banana orbits for it. Though a $z = 0$ surface of section is not the easiest way to view the development of this instability, it is a simple case of a supercritical pitchfork bifurcation. It is more common in SEP than in SED potentials in our survey because of the stronger z-dependence of the former for the same values of the flattening parameter q.

3.2.2. Period-tripling Bifurcations

FIGURE 2(a) shows the additional feature of a three-island chain. A new family of orbits has appeared because the three points at the center of the islands represent the successive crossings of the surface of section by the "reflected fish" orbit shown in FIGURE 2(c). This is a periodic orbit in which four oscillations in R are performed in the time that it takes to accomplish three oscillations in z. The other orbits of the family, represented by curves lying in the islands, fill a fatter region in $R - z$ space of the same characteristic shape.

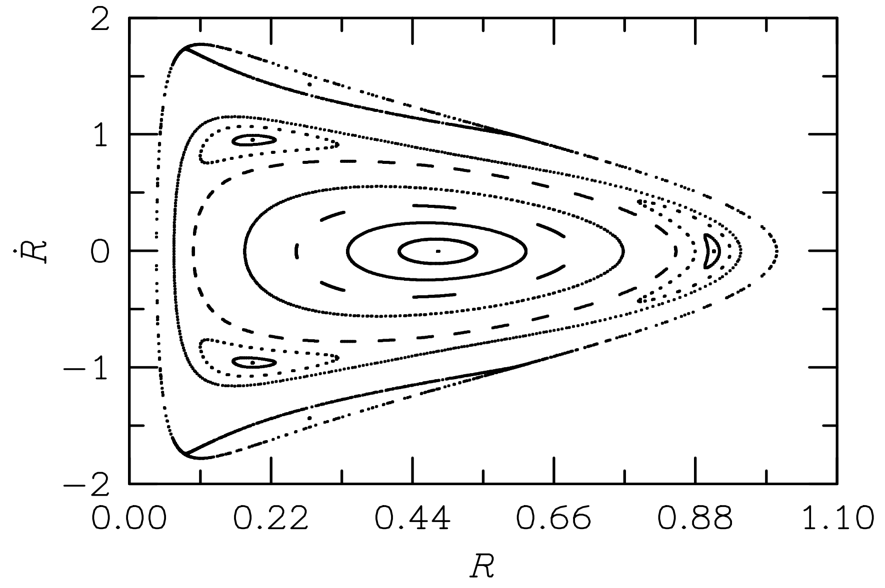
2
1
0
−1
−2
0.00
0.22
0.44
0.66
0.88
1.10
$\dot{R}$
R

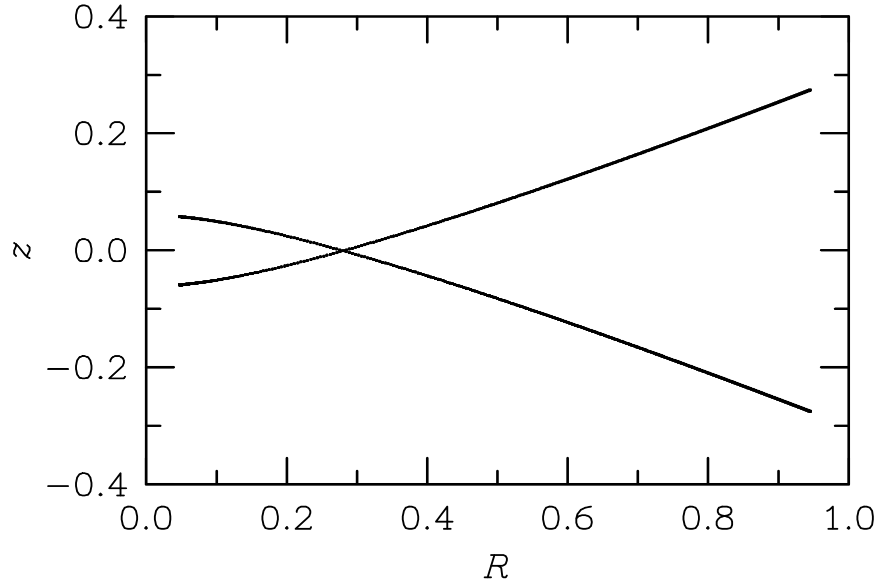
0.4
0.2
0.0
−0.2
−0.4
0.0
0.2
0.4
0.6
0.8
1.0
z
R

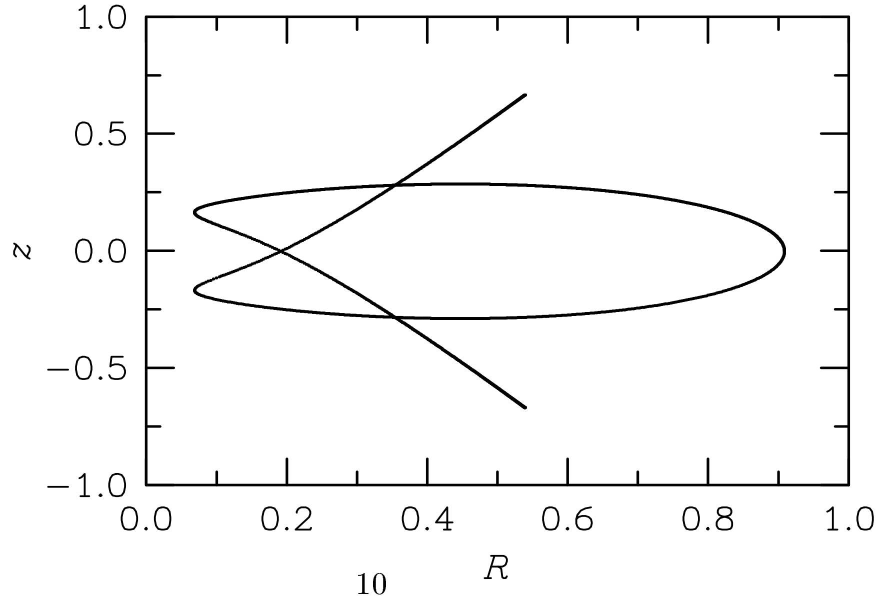
1.0
0.5
0.0
−0.5
−1.0
0.0
0.2
0.4
0.6
0.8
1.0
z
R

FIGURE 2. (**a**) The $(R, \dot{R})$ surface of section of an oblate SEP potential with $q = 0.8$, $\beta = -0.1$ at angular momentum $L_z^2 = 0.01$. It shows two bifurcations that have occurred; the equatorial plane orbit has become unstable, giving rise to the upper and lower islands, and a three-island chain has appeared. (**b**) The (R, z) paths of the pair of banana orbits that have bifurcated symmetrically from the equatorial plane orbit, and are represented by the central points of the upper and lower islands in FIGURE 2(a). (**c**) The (R, z) paths of the periodic 4:3 reflected fish orbit represented by the points at the centers of the three-island chain.

It has been suggested[1,9] that the three-island chains in a surface of section arise through a periodic tripling bifurcation of the central thin tube orbit when there is a 4:3 resonance between motions in R and those in z. We expended considerable effort trying to make this connection. Sometimes we seemed to be successful, as in the case illustrated in FIGURE 3(a). Note that the periodic orbit corresponding to the centers of the islands shown in FIGURE 3(b) differs in one respect from the reflected fish of FIGURE 2(c). It adds a four-fold oscillation in R and a three-fold one in z to a thin tube like that of FIGURE 1(b) which has two in-and-out oscillations in R for every one in z. The net result is the six oscillations in R for every three in z in FIGURE 3(b).

The fact that three-island chains can occur through some mechanism other than a bifurcation of the central thin tube orbit was made clear when careful and detailed integrations by Balša Terzić[10] caught not one, but two three-island chains, shortly after their creation at $L_z^2 = 0.022$ in an SED potential with $q = 0.8$, $\beta = 0.3$. That surface of section is shown in FIGURE 3 of his paper in this volume. No islands are visible in surfaces of section for slightly larger values of L_z^2, and it is apparent that two pairs of period-three orbits, one of each pair stable and the other unstable, are created in the outer regions of the surface of section and not at its central point. FIGURE 4 shows the similar shapes of one of these pairs, the pretzels. The other pair are reflected fish similar to that shown in FIGURE 2(c).

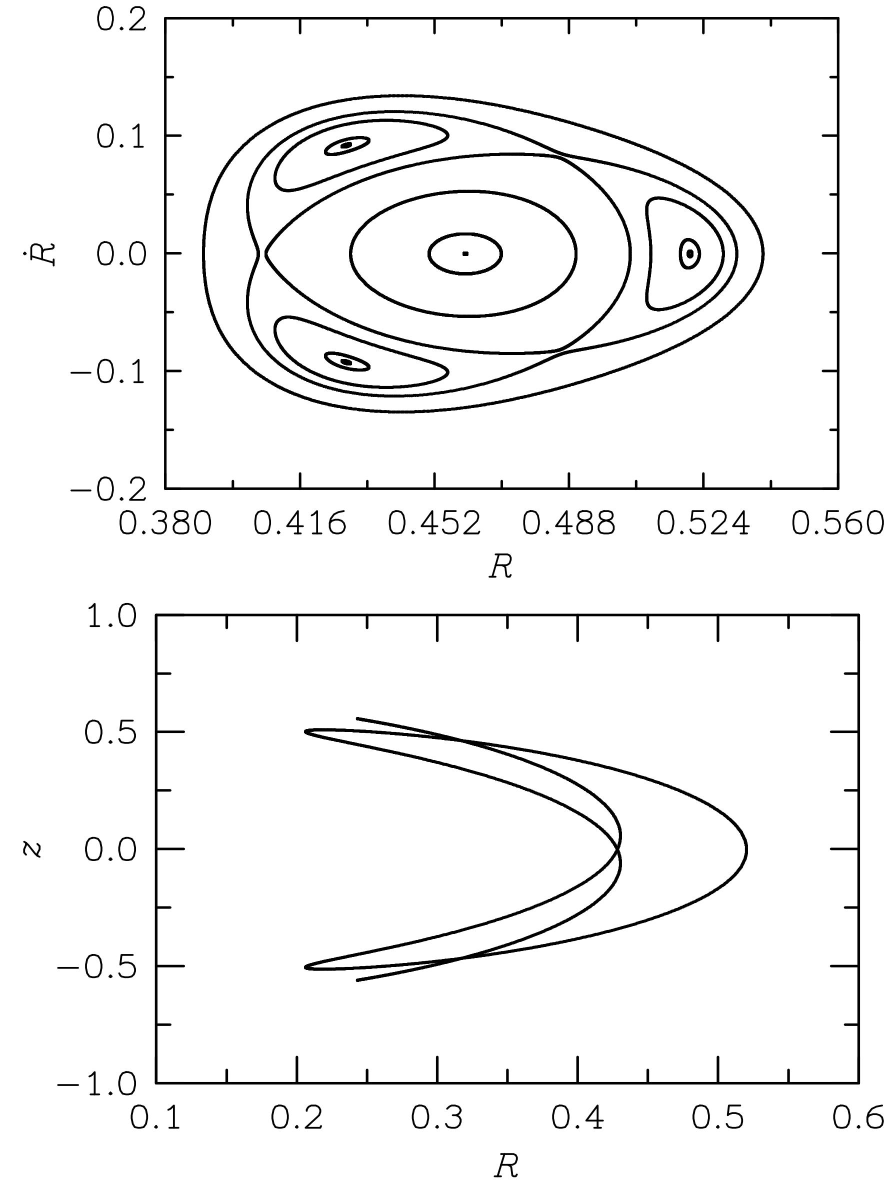

FIGURE 3. (**a**) The central part of the $(R, \dot{R})$ surface of section for a $q = 0.75$, $\beta = 0$, logarithmic SEP potential (7), in which a pair of period-three orbits has appeared near the center. The rotation angle, as defined in our Section 4, is $\alpha = 120.0123°$. (**b**) The (R, z) path of the stable period-three orbit represented by the centers of the three surrounding islands.

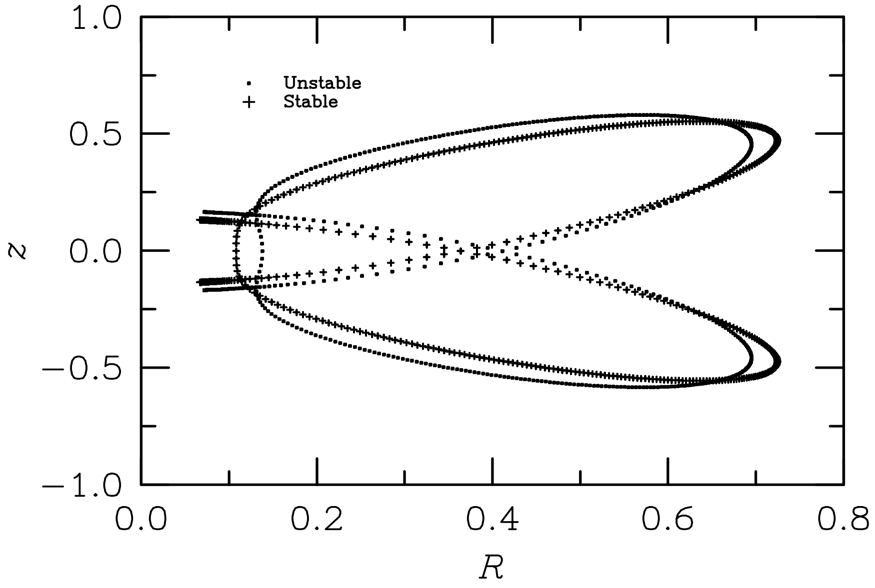

FIGURE 4. The (R, z) paths of the pretzel pair of period-three orbits, one stable and the other unstable. that occur at $L_z^2 = 0.222$ in an SED potential with $q = 0.8$, $\beta = 0.3$. The $(R, \dot{R})$ surface of section for this potential is that shown in Terzić FIGURE 3.[10]

Similar bifurcation phenomena are found with prolate SED potentials. The basic bifurcation-free surfaces of section are now more complex because there are two families of tube orbits, inner and outer tubes, characterized by whether their parent orbit crosses $z = 0$ when closest to, or furthest from, the z-axis. Both families are apparent in FIGURE 5(a), which shows also that a period-three orbit has arisen in the midst of the outer tube region. Its (R, z) path is shown in FIGURE 5(b); the tail of this reflected fish is bent back so that it has the same six oscillations in R to three in z as FIGURE 3(b). Period-three orbits also occur in the inner tube region. FIGURE 6 shows an instance from a different surface of section, for which the bifurcated orbit has a shape akin to that of an inner tube.

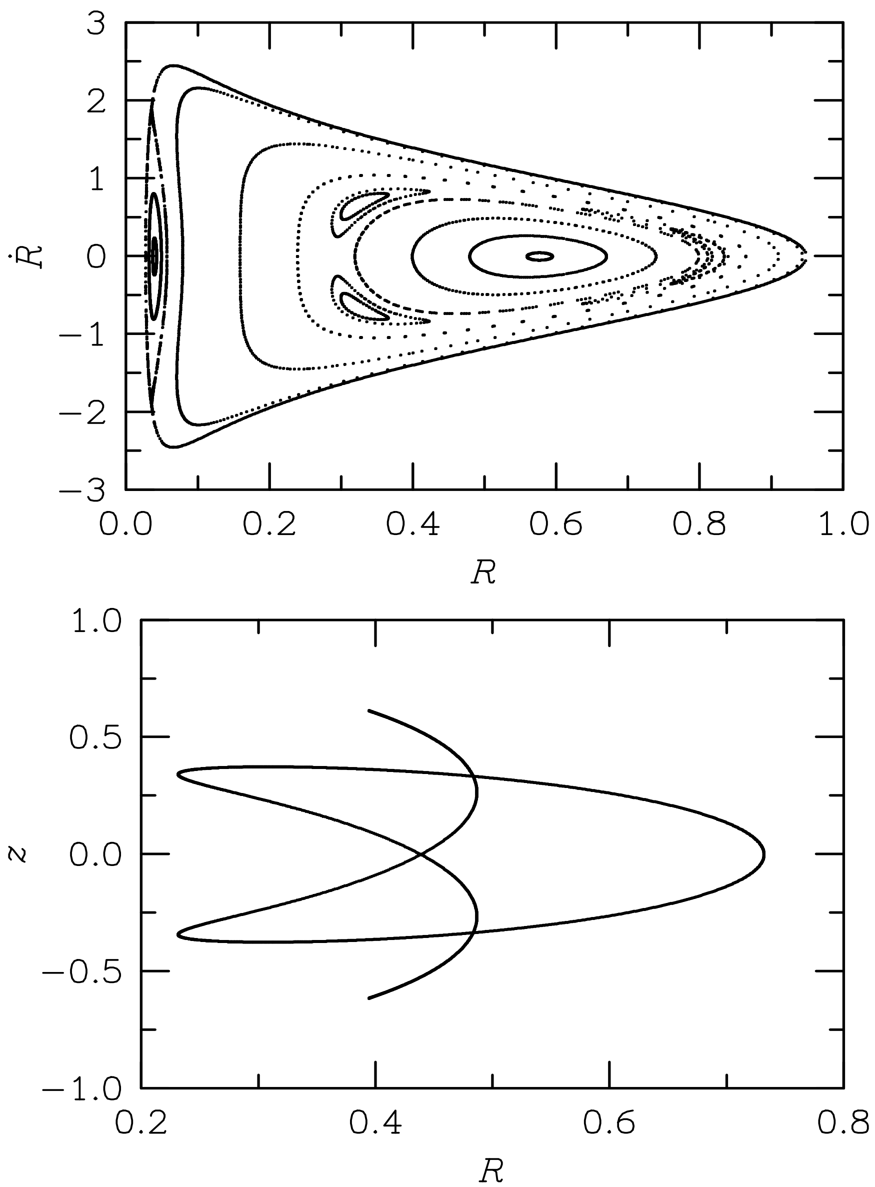

FIGURE 5. (**a**) The $(R, \dot{R})$ surface of section for the prolate SED potential with $q = 1.2$, $\beta = 0.1$ and $L_z^2 = 0.01$. The elongated narrow region to the left is occupied by inner tubes, while the larger region to the right is that of the outer tubes. A stable period-three orbit has appeared in the outer long axis tube region; its (R, z) path is shown in (**b**).

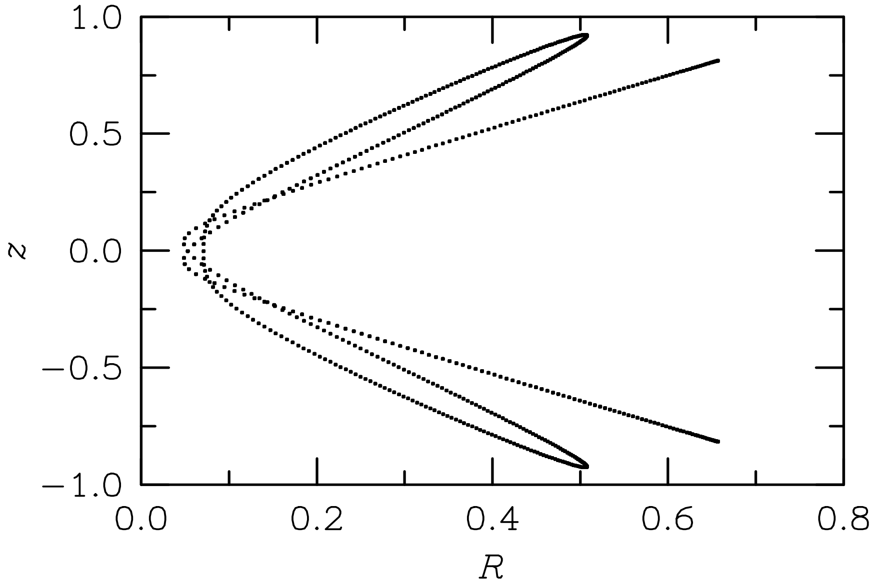

FIGURE 6. The (R, z) path of the stable period-three orbit which corresponds to the small three-island chain that closely surrounds the center of the inner tube region of the surface of section for the prolate SED potential with $q = 1.2$, $\beta = -0.1$, $L_z^2 = 0.004$. The surface of section is like that depicted in FIGURE 3(a), while the bifurcated orbit retains the characteristic shape of an inner tube.

3.2.3. Instability of the Thin Tube Orbit

The thin tube orbit can become unstable through a 1:1 resonance between radial and perpendicular motions, and this leads to the distinctive sequence of surfaces of section displayed in FIGURE 7. This phenomenon has been observed only in strongly flattened potentials; the $q = 0.4$ SED potential of FIGURE 7 corresponding to an E6 elliptical galaxy. There is first a supercritical pitchfork bifurcation as the thin tube, which is symmetric in z, is replaced with a pair of stable thin tubes which are not. The symmetric thin tube orbit soon regains its stability at a lower angular momentum through a subcritical pitchfork bifurcation, when an unstable period-one orbit is shed. This orbit follows a simple circuit in (R, z) space which is symmetric in z and which crosses the $z = 0$ plane at the two unstable fixed points in the surface of section; the outer one corresponding to a counterclockwise description of the circuit, and the inner one to a clockwise description. The stable pair of unsymmetric thin tube orbits which is formed at the first bifurcation from the symmetric thin tube persists unaffected by the second bifurcation. The families of the three stable orbits then grow to dominate the surface of section at yet lower angular momenta.

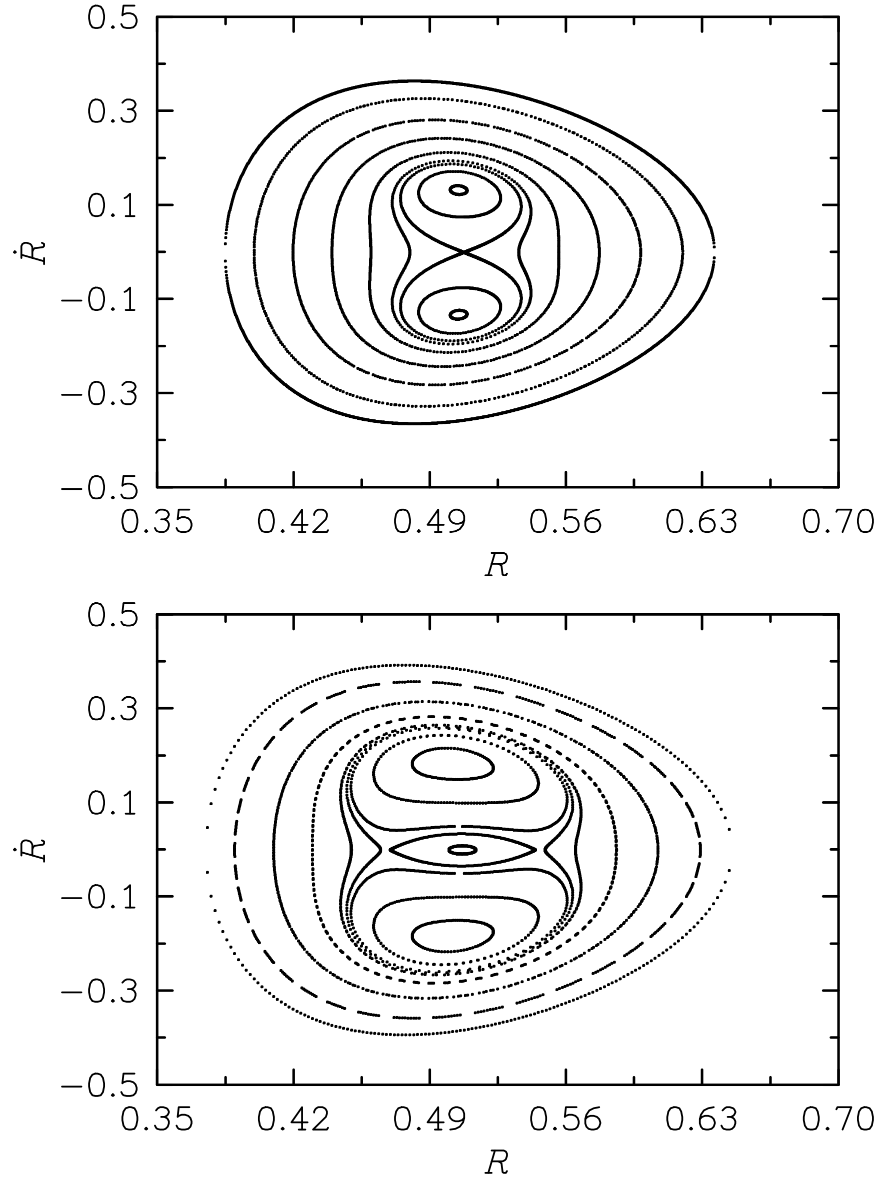

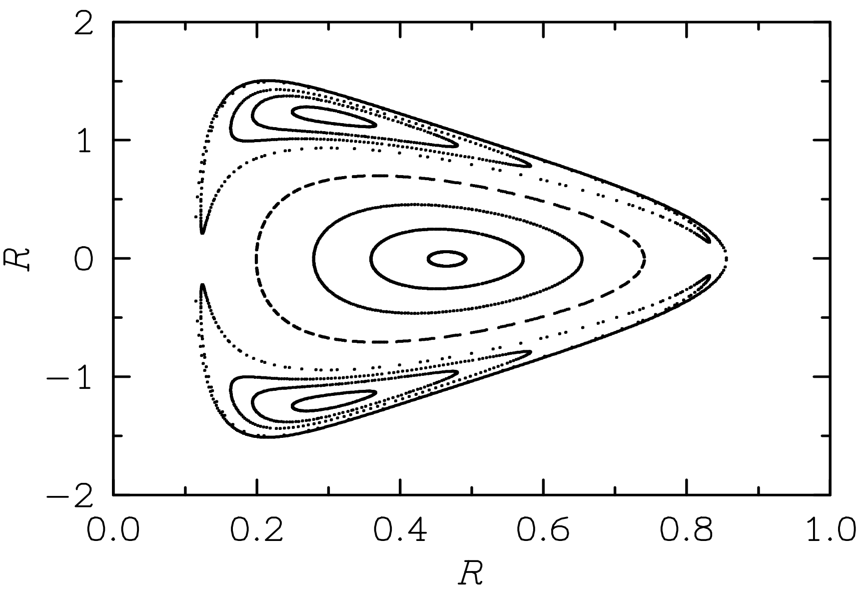

FIGURE 7. A sequence of $(R, \dot{R})$ surfaces of section at different angular momenta for the strongly flattened oblate SED potential with $q = 0.4$ and $\beta = 0.5$. The thin tube orbit becomes unstable to a 1:1 resonance and is replaced with a pair of stable orbits before (**a**) $L_z^2 = 0.335$. Then, before the stage (**b**) $L_z^2 = 0.33$ is attained even, the central thin tube has regained its stability. Subsequent surfaces of section at lower angular momenta, such as (**c**) $L_z^2 = 0.1$, have the same topology, but the families of the three stable orbits grow to dominate the surface of section. Note that this topology differs from those in which a pair of banana orbits has simply bifurcated from the equatorial plane orbit because of the connection between the upper and lower regions through the two unstable points on the R-axis.

3.2.4. Weakly Cuspy Stäckel Potentials

A family of scalefree potentials, with quite different orbital populations, are the weakly cuspy Stäckel potentials studied by Sridhar & Touma.[11] They form a one-parameter family with

$$\Phi = -\frac{1}{2\beta r^\beta} \left[(1+\cos\theta)^{1-\beta} + (1-\cos\theta)^{1-\beta} \right]. \tag{20}$$

There is now no second parameter q because the angular variation is fully determined by the parameter β. These potentials are only mildly cuspy because the parameter β is here limited to the range $-2 < \beta < -1$, well removed from that of our other models, by the requirements that density be everywhere positive and singular only at $r = 0$.

Like all Stäckel potentials, (20) has an exact third integral I_3 that is quadratic in the velocities. Hence $z = 0$ surfaces of section can be constructed analytically as contours of constant I_3. There are no tube orbits at any angular momentum, only banana orbits, so that the surface of section consists of two sets of concentric rings, one above and one below the R-axis, separated by this axis which represents the single unstable orbit in the plane, and surrounded by the bounding equatorial plane orbit. The banana orbits arise, as usual, from a 1:1 resonance because $\kappa = \nu$ for the potential (20).

Another remarkable property of the potential (20) is that it remains Stäckel when a central point mass $-GM/r$ term is added to it, though it is then no longer scalefree. In the limit of a dominant central mass, the third integral I_3 becomes the z-component of the Laplace-Runge-Lenz vector.[12]

4. MAPS AND THEIR BIFURCATIONS

4.1. Elliptic Fixed Points

Like many before us, we have sought to understand bifurcations through a study of maps that model the area-preserving map that takes one crossing of a surface of section to the next. We write this map in the form

$$\begin{bmatrix} x \\ y \end{bmatrix} \mapsto \begin{bmatrix} x' \\ y' \end{bmatrix} = \begin{bmatrix} F(x,y) \\ G(x,y) \end{bmatrix} \tag{21}$$

for some functions F and G, aligning the x- and y-axes with the R and $\dot{R}$ axes of our surfaces of section respectively. Our goal is to study the process through which period-three orbits and their accompanying three-island chains arise.

To study the behavior in the neighborhood of the elliptic fixed point that represents the thin tube orbit, we place our origin there. We expand the map, which we assume to be locally analytic, about the fixed point in the form

$$\begin{bmatrix} x \\ y \end{bmatrix} \mapsto \begin{bmatrix} x' \\ y' \end{bmatrix} = \begin{bmatrix} x\cos\alpha + y\sin\alpha + \dots \\ -x\sin\alpha + y\cos\alpha + \dots \end{bmatrix}, \tag{22}$$

with the dots signifying higher order terms. A rescaling to make the invariant ellipses circular, such as $x = R - R_0$, $y = \dot{R}/\kappa$ in (19), is the only transformation necessary in this case to reduce the linear part of the map (21) to the simple rotation form in (22). Our rotational angle α, which is in the opposite sense from that usually chosen, is a natural choice here with $\alpha = 2\pi\kappa/\nu$ for (19).

A compact and convenient way of representing the expanded form of (22) is the complex form

$$z' = x' + iy' = e^{-i\alpha}z + az^2 + bz\,\overline{z} + c\overline{z}^2 + \dots\ . \tag{23}$$

for some constants a, b and c. Siegel and Moser[13] prove that, if $e^{-3i\alpha} = 1$, as it is when $\kappa/\nu = 4/3$ and there is a 4:3 resonance between radial and perpendicular motions, *and* $c \neq 0$, then the fixed point at $(0,0)$ is unstable. In our survey we study a sequence of surfaces of section that change as a parameter such as L_z^2 is varied. The angle then α varies continuously and this instability is momentary. A more significant result therefore is that of Meyer & Hall[14] who prove that the orbit of period three, which, with varying α, bifurcates from the fixed point at O when $e^{-3i\alpha} = 1$, consists of three hyperbolic points. FIGURE A.6 of their Chapter VIII illustrates this process schematically, and Hale & Koçak's[15] FIGURE 15.18 shows it in detail for an area-preserving Cremona map. No three-island chains, such as we see in our FIGURE 3(a) are formed.

4.2. Generating Functions

Maps are guaranteed to be exactly area-preserving if they are derived from generating functions. As in mechanics[12], the generating function combines an old and a new variable. We shall use a generating function of the form $W(x, x')$ to define an area-preserving map according to relations

$$y = \frac{\partial W}{\partial x}, \quad y' = -\frac{\partial W}{\partial x'}. \tag{24}$$

We require also that the map incorporate the following symmetry that is present in our orbital dynamics. Orbits can be reversed in time and run backwards because our potentials are time-independent. Reversing time changes $\dot{z} > 0$ crossings of $z = 0$ into $\dot{z} < 0$ ones, which are not the crossings that our surfaces of section record. However, every reversed orbit has a mirror image twin (reflected in the $z = 0$ plane) because our potentials are even in z, and this has $\dot{z} > 0$ in place of $\dot{z} < 0$ crossings of $z = 0$. The mathematical expression of this combination of time reversibility and symmetry in z is the requirement that the map satisfy the condition

$$\begin{bmatrix} x' \\ -y' \end{bmatrix} \mapsto \begin{bmatrix} x \\ -y \end{bmatrix}.$$

This condition implies that $W(x, x')$ is symmetric in its arguments. We now define $Q(x, x') = \partial W/\partial x$, and write the map as

$$y = Q(x, x'), \quad y' = -Q(x', x). \tag{25}$$

4.3. Orbits of Period Three

An orbit of period three

$$\begin{bmatrix} x_0 \\ y_0 \end{bmatrix} \mapsto \begin{bmatrix} x_1 \\ y_1 \end{bmatrix} \mapsto \begin{bmatrix} x_2 \\ y_2 \end{bmatrix} \mapsto \begin{bmatrix} x_0 \\ y_0 \end{bmatrix},$$

of the map (25) requires a solution of the system

$$\begin{gathered} y_0 = Q(x_0, x_1), \quad y_1 = Q(x_1, x_2), \quad y_2 = Q(x_2, x_0), \\ y_1 = -Q(x_1, x_0), \quad y_2 = -Q(x_2, x_1), \quad y_0 = -Q(x_0, x_2). \end{gathered} \tag{26}$$

A non-trivial and generic possibility is

$$y_0 = 0, \quad x_2 = x_1, \quad y_2 = -y_1, \tag{27}$$

which is achieved if some solution, other than $x_0 = x_1$, can be found of the pair of simultaneous equations

$$Q(x_0, x_1) = 0, \quad Q(x_1, x_1) + Q(x_1, x_0) = 0. \tag{28}$$

The $x_0 = x_1$ case can be eliminated by combining equations (28) in the form

$$Q(x_1, x_1) + Q(x_1, x_0) - 2Q(x_0, x_1) = 0, \tag{29}$$

and then explicitly eliminating the $(x_0 - x_1)$ factor.

4.4. A Cubic Generating Function

We now select a class of generating functions for studying how and when orbits of period three arise. We study the general symmetric cubic W,

$$W(x, x') = \frac{xx' - \frac{1}{2}(x^2 + x'^2)\cos\alpha}{\sin\alpha} + [I_1(x^3 + x'^3) + I_2 xx'(x + x')]. \tag{30}$$

Its quadratic terms give the linear part of (22), while the additional cubic terms introduce nonlinear effects. This form of generating function is inappropriate for analyzing the bifurcations related to $\alpha = 0$ or $\alpha = 180°$, but that is not our concern. We restrict attention to $0 < \alpha < 180°$ since maps for $0 > \alpha > -180°$ are simply reflections of ones we consider. Because scaling transformations do not alter the map in any significant way, the constants multiplying the cubic terms in (30) can be scaled so that they depend on a single parameter. We therefore introduce a polar representation and write

$$I_1 = \cos\gamma, \quad I_2 = \sin\gamma. \tag{31}$$

Because of symmetries, we can restrict γ to the range $0 \leq \gamma \leq 180°$, which leaves us with a $180° \times 180°$ box of (α, γ) parameter space to survey. Our map is explicit only in the special case of $I_2 = \sin\gamma = 0$. Otherwise we solve $y = \partial W/\partial x$, which is a quadratic for x', by selecting the root that $\to 0$ as $(x, y) \to 0$. The algebra is elementary - see Appendix A.2 for some details - with (29), which is the only possibility in this case, reducing to a linear relation between x_0 and x_1. The results confirm that, generically, orbits of period three are created as a pair, one unstable and the other unstable, at a triad of distinct points (27). This happens through a turning point bifurcation, as captured in Terzić's[10] FIGURE 3, except that two pairs form there whereas only one pair ever forms with the present model. When γ is held fixed and α is increased, a pair of period-three orbits is created at values $\alpha = \alpha_{\text{crit}}$ which are included in the plot shown in FIGURE 8.

Only unstable period-three orbits are found for the range $80.54° < \gamma < 111.43°$ for which values of α_{crit} are missing. The critical rotation angle α_{crit} never exceeds $120°$, and is $120°$ only for $\gamma = \tan^{-1} 2 = 63.43°$, when the constant $c = 0$ in the expansion of (23) so that Siegel and Moser's[13] instability result does not apply. Otherwise α_{crit} is close to $120°$ over a wide range. Stable period-three orbits are rare because they exist in only a small portion of the parameter space of FIGURE 8. Except in a narrow band to the immediate right of $\gamma = 111.43°$, the stable period-three orbit has only a short span of existence, a few degrees in α, before it becomes unstable through a supercritical pitchfork bifurcation corresponding to a period-doubling instability. The generic bifurcation diagram for fixed γ and varying α is shown in FIGURE 9. Note that it is the unstable period-three orbit that passes through the fixed point at $(0, 0)$ at $\alpha = 120°$, which conforms with the result of Meyer and Hall[14]. FIGURE 10(a) shows the $\alpha = 120°$ map for $\gamma = 65°$ for which $\alpha_{\rm crit} = 119.97°$. The stable period-three orbit is evident there at the stage that the unstable one has momentarily destabilized the elliptic fixed point at O. FIGURE 10(b) at $\alpha = 122°$ shows the stability of the elliptic fixed point at O restored, and stable and unstable period-three orbits around it, qualitatively similar to the surface of section of FIGURE 3(a).

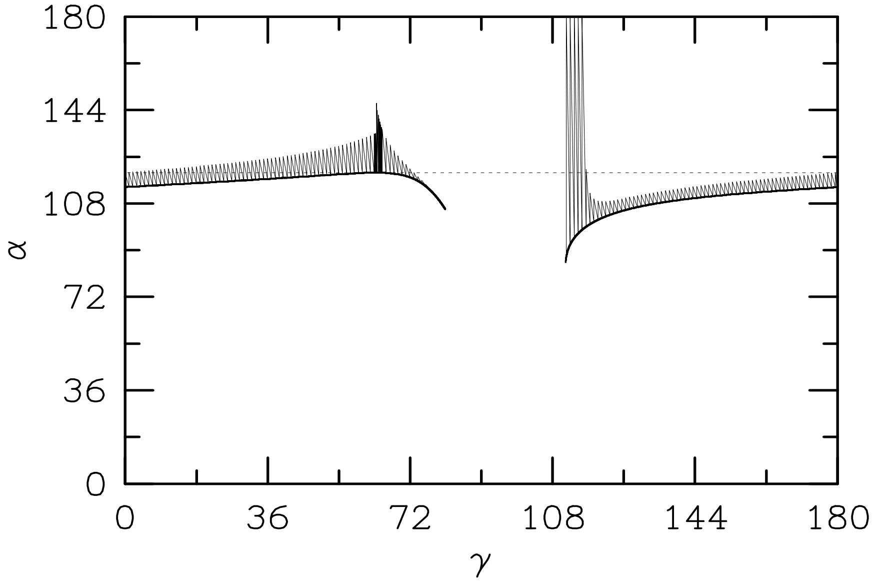

FIGURE 8. The two shaded regions display the portions of (γ, α) space in which the map generated by (30) has stable period-three orbits. The regions are bounded below by the solid curve which corresponds to the critical rotation angle $\alpha_{\rm crit}$ at which a pair of period-three orbits, one unstable and the other unstable, is created. They are bounded above by the occurrence of a destabilizing period-doubling bifurcation.

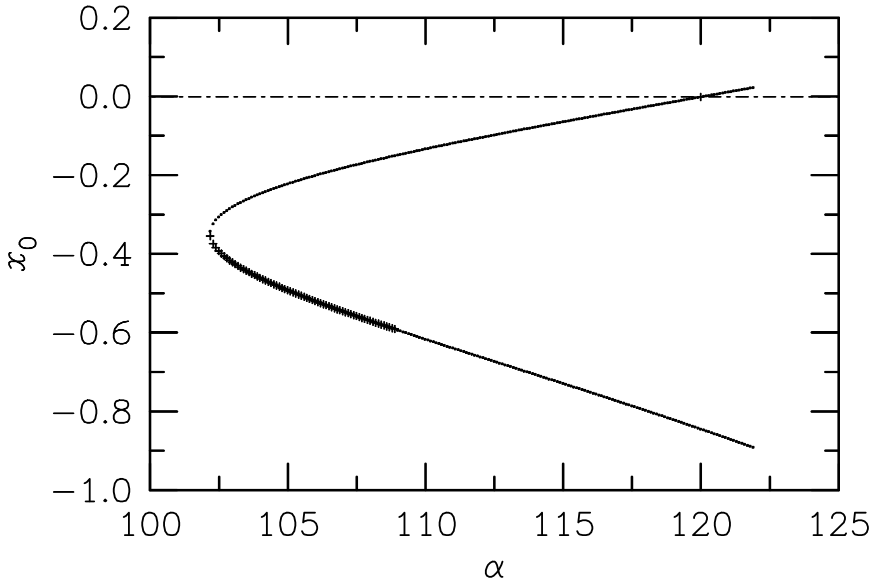

FIGURE 9. The generic bifurcation diagram, for fixed γ and varying α, for period-three orbits, showing how x_0, the x-coordinate of the point of the orbit on the y-axis, varies with α. The specific case plotted is that of $\gamma = 120°$. The crosses, which form the thicker segment, mark the range of stable period-three orbits, while the dot–dash line marks the period-one fixed point. The diagram is reversed, and the values of x_0 positive for stable period-three orbits as in FIGURE 3(a), when $\gamma < \tan^{-1} 2$.

Hénon[16] studied the most general quadratic map that is area-preserving and explicit,

$$x' = x\cos\alpha + (y - x^2)\sin\alpha,$$

$$y' = x\sin\alpha + (y - x^2)\cos\alpha.$$

(We have changed the sign of his α to conform with our usage.) Although not explicitly time-reversible, Hénon's map can be obtained by transformation from a time-reversible DeVogelaere map[17]; that is a map with a generating function $W = W_1(x) + W_1(x')$ in our notation. Hénon found that as α increased, a pair of orbits of period three are created together at $\alpha = \cos^{-1}(1 - \sqrt{2}) = 114.47°$. The unstable orbit passes through O at $\alpha = 120°$, at which stage the stable orbit loses its stability. Hénon's map is equivalent to the special $I_2 = 0$ case for which our map becomes explicit; the requirement of explicitness greatly reducing the variety of time-reversible maps that can be obtained from a generating function.

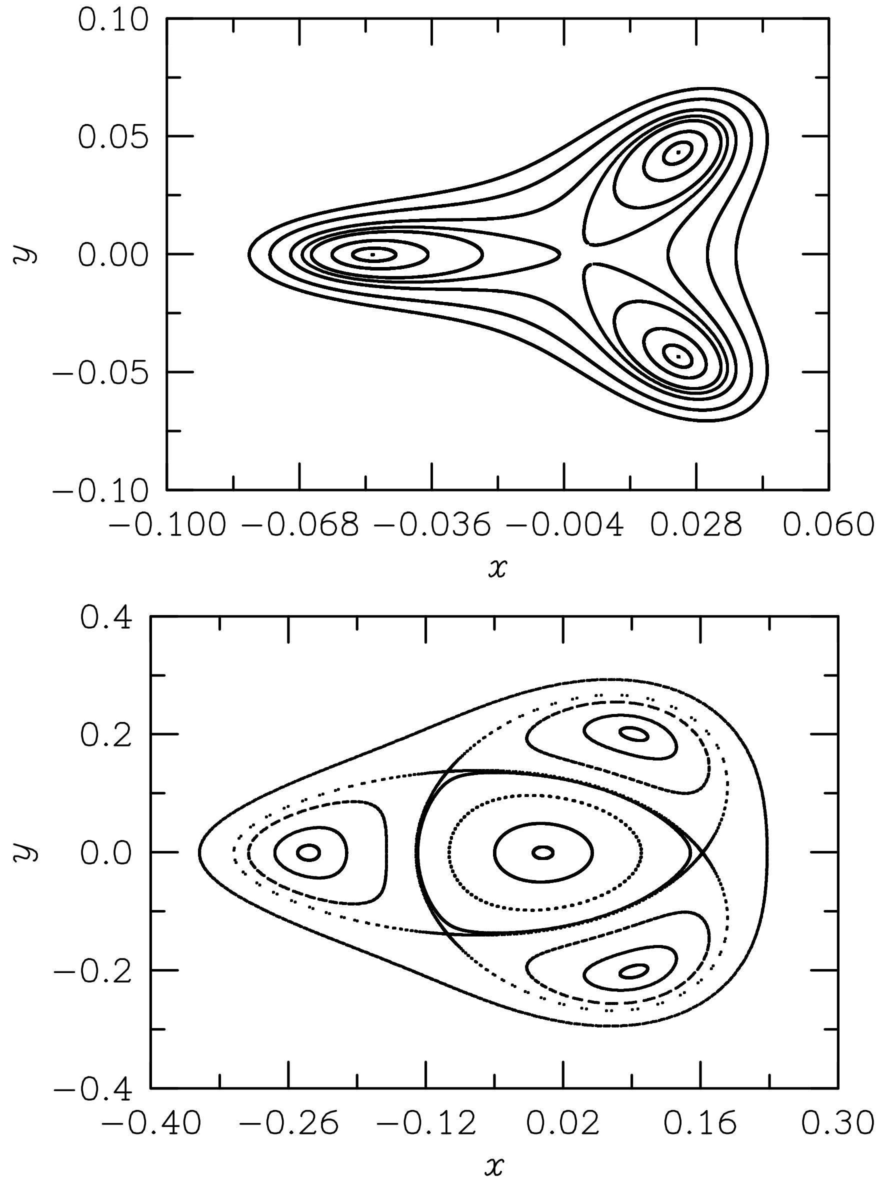

FIGURE 10. Two cases of the map generated by (30) for $\gamma = 65°$. (**a**) At $\alpha = 120°$, the unstable period-three orbit has collapsed to the fixed point at O which becomes momentarily unstable. There is a stable period-three orbit present too. (**b**) At $\alpha = 122°$, the fixed point at O has restabilized, the unstable period-three orbit has re-emerged, and the stable period-three orbit is still present.

5. DISCUSSION AND CONCLUSIONS

This has been a selective and incomplete study of bifurcations of periodic orbits in axisymmetric scalefree potentials with central cusps. It has focussed on the most prominent bifurcations, and especially on the less understood orbits of period three in their crossing of the central plane. The figures we display are selected to highlight instances of bifurcations. Many surfaces of section, especially ones for spheroidal equidensity (SED) potentials, are duller, showing only tube orbits and no prominent bifurcations.

The family of maps introduced in Section 4 gives some significant insights. It is derived from a generating function which is of general type for problems with the same symmetries as ours, and which is truncated consistently at cubic terms. Hence it should encompass all phenomena that generally arise sufficiently close to an elliptic fixed point. Our analysis shows that its stable period-three orbits generically arise away from an elliptic fixed point through a turning-point bifurcation. Only exceptionally does a stable period-three orbit arise from a bifurcation of an elliptic fixed point when its rotation angle passes through 120°. However there is a wide parameter range in which the turning-point bifurcation occurs when the rotation angle is close to 120°, which can explain why stable period-three orbits are often found quite close to the elliptic fixed point. On the other hand, there are none to be found in other parameter ranges. That, plus the generally short range between the stages at which a stable period-three orbit arises and that at which it becomes unstable, is consistent with the scarcity of three-island chains found in surfaces of section. All of these period-three orbits belong to what Contopoulos[18] classifies as a regular family in that they are all connected, as in the bifurcation diagram of FIGURE 9, to the basic thin tube orbit. A more elaborate map and high order map than our equations (24) and (30) allows is needed to account for the creation of the two pairs of irregular period-three orbits that Terzić's[10] remarkable FIGURE 3 shows.

ACKNOWLEDGMENTS

It is no surprise that many of the phenomena described in this work are already known to George Contopoulos, this meeting's honoree. In addition to his earlier classification of families of periodic orbits as either regular or irregular, Contopoulos and Michaelidis[19] studied the specific problem of the bifurcations of triple-periodic orbits in the context of the two-dimensional potential $\Phi(x, y) = \frac{1}{2}(\omega_1^2 x^2 + \omega_2^2 y^2) - \varepsilon x y^2$ as the parameter ε is

increased. Their FIGURE 2(a) plots what at first appears to be a stable and an unstable period-three orbit bifurcating from a stable period-one orbit. The closer analysis shown in their magnified FIGURE 2(b) reveals that this is not so, and that the two period-three orbits are in fact created as a pair slightly away from the period-one orbit. The unstable period-three orbit then passes through the period-one orbit as in our FIGURE 9. These instances serve to remind us of some of the many ways in which George has been a pioneer in the understanding of dynamical phenomena. We appreciate the privilege of being invited to this meeting and of being able to contribute this paper in his honor.

APPENDIX

A.1. Computing Surfaces of Section

Here we present the simple method which we have used for computing crossings of a surface of section without any need for interpolation, and without losing any of the accuracy of a high order ODE solver. Like Hénon[20], we accomplish this by using an independent variable whose value at the surface of section is known. Unlike Hénon, we use that same independent variable throughout the integration. To be specific, we introduce polar coordinates A and ψ in the $(z, \dot{z})$-plane, via the transformations

$$z = A \sin\psi, \quad \dot{z} = A\cos\psi, \tag{32}$$

where the amplitude A is to be always positive. We use ψ, rather than time, as the variable of integration. Then the crossings of the $z = 0$ surface-of-section occur at $\psi = n\pi$ for integer n, and the crossings with $\dot{z} > 0$, which are the ones we record, occur for even values of n.

Differentiation of equations (32) gives

$$\begin{aligned} \dot{z} &= A\dot{\psi}\cos\psi + \dot{A}\sin\psi = A\cos\psi, \\ \ddot{z} &= -A\dot{\psi}\sin\psi + \dot{A}\cos\psi = -\nu^2 z = -\nu^2 A\sin\psi, \end{aligned} \tag{33}$$

where ν is now defined as the local frequency in the z-direction

$$\nu^2(R, z) = \frac{1}{z}\frac{\partial\Phi}{\partial z}. \tag{34}$$

This reduces to the earlier definition of (18) in the limit of $z \to 0$. Equations (33) can be solved to give the equations

$$\overset{\bullet}{A} = A(1-\nu^2)\sin\psi\cos\psi, \quad \overset{\bullet}{\psi} = \cos^2\psi + \nu^2\sin^2\psi. \tag{35}$$

The first of these equations shows that an initially positive A cannot become zero in finite time and hence remains positive if it is so initially. The second shows that ψ is always an increasing function of t, and so can be used as the independent variable of integration. The integration needed is that of the following first order system of three equations for the three unknowns A, R, and $\overset{\bullet}{R}$,:

$$\frac{dA}{d\psi} = \frac{\overset{\bullet}{A}}{\overset{\bullet}{\psi}}, \quad \frac{dR}{d\psi} = \frac{\overset{\bullet}{R}}{\overset{\bullet}{\psi}}, \quad \frac{d\overset{\bullet}{R}}{d\psi} = \frac{\ddot{R}}{\overset{\bullet}{\psi}}. \tag{36}$$

Their right hand sides are all known functions of A, ψ, R, and $\overset{\bullet}{R}$ because $z = A\sin\psi$. We integrate from a starting point (R_0, V_0) in an $(R, \overset{\bullet}{R})$ surface of section using the initial conditions

$$\psi = 0, \quad A = \sqrt{2E - \frac{L_z^2}{R_0^2} - 2\Phi(R_0, 0) - V_0^2}, \quad R = R_0, \quad \overset{\bullet}{R} = V_0. \tag{37}$$

A.2. Period-three Orbits of the Map generated by (30)

The Q function for the map (25) is

$$Q(x, x') = \frac{x' - x\cos\alpha}{\sin\alpha} + 3x^2\cos\gamma + x'(2x + x')\sin\gamma. \tag{38}$$

Elimination of the y_i between equations (26) then shows that one pair of x_i must coincide, and hence that (27) is now the only possibility for period-three orbits. Eliminating the $(x_0 - x_1)$ factor from equation (29) gives the condition

$$(6\cos\gamma - \sin\gamma)x_0 + (6\cos\gamma + \sin\gamma)x_1 = \frac{2\cos\alpha + 1}{\sin\alpha}.$$

Using this condition to eliminate x_1 from the equation $Q(x_0, x_1) = 0$ gives a quadratic for x_0, and hence two *possible* period-three orbits. They are not *valid* period-three orbits unless each step of the map satisfies the condition

$$x' = \frac{-(1+2x\sin\alpha\sin\gamma)+\sqrt{[1+2x\sin\alpha\sin\gamma]^2-4\sin\alpha\sin\gamma[(3x^2\cos\gamma-y)\sin\alpha-x\cos\alpha]}}{2\sin\alpha\sin\gamma}, \tag{39}$$

that is necessary for $(0,0)$ is to be a fixed point.

Orbits of period three are created, where none are present before, at a stage at which the two roots of the quadratic for x_0 cease to be complex conjugate pair and become equal. That stage occurs for

$$(2\lambda^2-1)\cos^2\alpha_{\text{crit}} - 2\cos\alpha_{\text{crit}} + \frac{1}{2}(\lambda+1)^2 - 1 = 0 \tag{40}$$

where

$$\lambda = \frac{\tan\gamma - 6}{\tan\gamma + 6}.$$

The roots of the quadratic (40) for $\cos\alpha_{\text{crit}}$ are complex when $\lambda > 1$ and when $\lambda < -2.47569$, the real root of the cubic $2\lambda^3+6\lambda^2+3\lambda+1=0$. Otherwise, there is just one feasible real root for $\cos\alpha_{\text{crit}}$ which lies in the range $[-\frac{1}{2},1)$ for $-1.4<\lambda<1$, but two in the range $(-\frac{1}{2},0)$ for $-2.47569<\lambda<-1.4$.

We now relate these properties to FIGURE 8. As γ increases from 0 on its left branch, λ increases from -1 and we are in the region of one real root for $\cos\alpha_{\text{crit}}$. The maximum value $\alpha_{\text{crit}} = 120°$, $\cos\alpha_{\text{crit}} = -\frac{1}{2}$, is attained only for $\lambda = -\frac{1}{2}$, that is for $\tan\gamma = 2$. Otherwise α_{crit} is less than 120° because the left hand side of (40) evaluated for $\cos\alpha_{\text{crit}} = -\frac{1}{2}$ is $(\lambda+\frac{1}{2})^2$ and so vanishes for $\lambda = -\frac{1}{2}$ only. The left branch of FIGURE 8 ends at $\gamma = \tan^{-1} 6$ where $\lambda = 0$ and $\alpha_{\text{crit}} = \cos^{-1}(2^{-1/2}-1) = 107.03°$. This is a stage at which the term in the square root of equation (39) vanishes when evaluated for $(x,y) = (x_0,0)$. It marks a transition beyond which the roots for α_{crit} found for yet larger values of γ no longer give valid period-three orbits because the condition (39) is not satisfied.

The left end of the right branch of α_{crit} values in FIGURE 8 lies at $\gamma = 111.43°$ where $\lambda = -2.47569$. The value of x_0 is infinite at this starting-point. Moving to its right, λ is again negative and increasing, and the quadratic (40) has two feasible roots for $\cos\alpha_{\text{crit}}$ as γ increases up until $\gamma = 135°$ when $\lambda = -1.4$. However, only the smaller value of these with the larger value of α_{crit} gives a valid period-three orbit. It continues to do so up to $\gamma = 180°$.

REFERENCES

1. Evans, N.W. 1994. Mon. Not. R. Astron. Soc. **267**: 333–360.

2. Lauer, T.R. *et al.* 1995. Astron. J. **110**: 2622-2654.

3. Qian, E.E., P.T. de Zeeuw, R.P. van der Marel, & C. Hunter. 1995. Mon. Not. R. Astron. Soc. **274**: 602–622.

4. Richstone, D.O.. 1982. Astrophys. J. **252**: 496-507.

5. Binney,J. & S. Tremaine. 1987. Galactic Dynamics. Chapter 3. Princeton Univ. Press. Princeton, NJ.

6. Chandrasekhar, S. 1969. Ellipsoidal Figures of Equilibrium, Chapter 3. Yale Univ Press. New Haven, CT.

7. Isaacson, E. & H.B. Keller. 1966. Analysis of Numerical Methods, Chapter 7. John Wiley. New York, NY.

8. Davis, P.J. 1975. Interpolation and Approximation, Chapter 12. Dover. New York, NY.

9. Lees, J.F. & M. Schwarzschild. 1992. Astrophys. J. **384**: 491–501.

10. Terzić, B. 1998. Ann. New York Acad. Sci. **000**: 000–000. (this volume).

11. Sridhar, S. & J. Touma. 1997. Mon. Not. R. Astron. Soc. **292**: 657–661.

12. Goldstein, H. 1980. Classical Mechanics. 2nd edit. Chapters 3 and 9. Addison-Wesley. Reading, MA.

13. Siegel, C.L. & J.K. Moser. 1971. Lectures on Celestial Mechanics. Section 31. Springer Verlag. New York.

14. Meyer, K.R. & G.R. Hall. 1992. Introduction to Hamiltonian Dynamical Systems and the N–Body Problem. Chapter VIII. Springer Verlag. New York.

15. Hale, J. & H. Koçak. 1991. Dynamics and Bifurcations. Springer Verlag. New York.

16. Henon, M. 1969. Quart. App. Math. **37**: 291-312.

17. Greene, J.M., R.S. MacKay, F. Vivaldi, & M.J. Feigenbaum. 1981. Physica D. **3**: 468–486.

18. Contopoulos, G. 1970. Astron. J. **75**: 96–107.

19. Contopoulos, G. & P. Michaelidis. 1980. Celest. Mech. **22**: 403–413.

20. Hénon, M. 1982. Physica D. **5**: 412–414.